AIP | Review of Scientific Instruments

# Momentum spectrometer for electron-electron coincidence studies on superconductors

Robert Wallauer, Stefan Voss, Lutz Foucar, Tobias Bauer, Deborah Schneider et al.

Citation: Rev. Sci. Instrum. **83**, 103905 (2012); doi: 10.1063/1.4754470
View online: http://dx.doi.org/10.1063/1.4754470
View Table of Contents: http://rsi.aip.org/resource/1/RSINAK/v83/i10
Published by the American Institute of Physics.

## Related Articles

New beam line for time-of-flight medium energy ion scattering with large area position sensitive detector
Rev. Sci. Instrum. 83, 095107 (2012)

Position and energy-resolved particle detection using phonon-mediated microwave kinetic inductance detectors
Appl. Phys. Lett. 100, 232601 (2012)

High-resolution Thomson parabola for ion analysis
Rev. Sci. Instrum. 82, 113504 (2011)

The response of CR-39 nuclear track detector to 1–9 MeV protons
Rev. Sci. Instrum. 82, 103303 (2011)

Increasing the energy dynamic range of solid-state nuclear track detectors using multiple surfaces
Rev. Sci. Instrum. 82, 083301 (2011)

## Additional information on Rev. Sci. Instrum.

Journal Homepage: http://rsi.aip.org
Journal Information: http://rsi.aip.org/about/about_the_journal
Top downloads: http://rsi.aip.org/features/most_downloaded
Information for Authors: http://rsi.aip.org/authors

ADVERTISEMENT

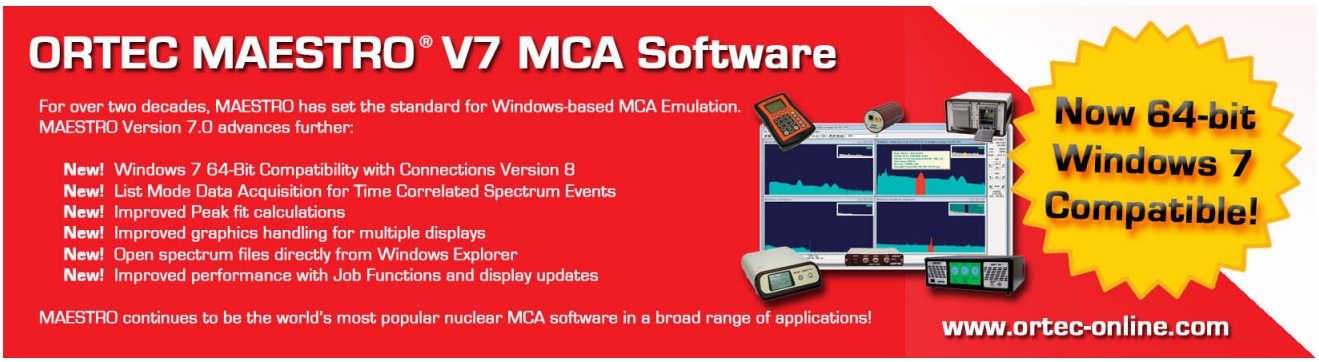

# Momentum spectrometer for electron-electron coincidence studies on superconductors

Robert Wallauer,[1,a)] Stefan Voss,[1] Lutz Foucar,[2,3] Tobias Bauer,[1] Deborah Schneider,[1] Jasmin Titze,[1] Birte Ulrich,[1] Katharina Kreidi,[1] Nadine Neumann,[1] Tilo Havermeier,[1] Markus Schöffler,[1] Till Jahnke,[1] Achim Czasch,[1] Lothar Schmidt,[1] Amit Kanigel,[4] Juan Carlos Campuzano,[5] Harald Jeschke,[6] Roser Valenti,[6] Andreas Müller,[7] Götz Berner,[7] Michael Sing,[7] Ralph Claessen,[7] Horst Schmidt-Böcking,[1] and Reinhard Dörner[1]

[1]*Institut für Kernphysik, Universität Frankfurt, Max-von-Laue-Str. 1, 60438 Frankfurt/Main, Germany*
[2]*Max Planck Advanced Study Group, Center for Free Electron Laser Science (CFEL), Notkestraße 85, 22607 Hamburg, Germany*
[3]*Max-Planck-Institut für medizinische Forschung, Jahnstraße 29, 69120 Heidelberg, Germany*
[4]*Technion, Technion City, 32000 Haifa, Israel*
[5]*University of Illinois at Chicago, 601 S. Morgan St., Chicago, Illinois 60607, USA*
[6]*Institut für Theoretische Physik, Universität Frankfurt, Max-von-Laue-Str. 1, 60438 Frankfurt/Main, Germany*
[7]*Physikalisches Institut, Universität Würzburg, Am Hubland, 97074 Würzburg, Germany*

(Received 10 August 2012; accepted 9 September 2012; published online 10 October 2012)

We present a new experimental setup to study electron-electron coincidences from superconducting surfaces. In our approach, electrons emitted from a surface are projected onto a time- and position-sensitive microchannel plate detector with delayline position readout. Electrons that are emitted within 2 $\pi$ solid angle with respect to the surface are detected in coincidence. The detector used is a hexagonal delayline detector with enhanced multiple hit capabilities. It is read out with a Flash analog-to-digital converter. The three-dimensional momentum vector is obtained for each electron. The intrinsic dead time of the detector has been greatly reduced by implementing a new algorithm for pulse analysis. The sample holder has been matched to fit the spectrometer while being capable of cooling down the sample to 4.5 K during the measurement and heating it up to 420 K for the cleaning procedure. © *2012 American Institute of Physics*. [http://dx.doi.org/10.1063/1.4754470]

## I. INTRODUCTION

Ejection of two electrons by absorption of a single photon ($(\gamma, 2e)$) is a highly sensitive probe of electron-electron correlation. It is used with great success in studies of gas phase atoms (e.g., see Ref. 1) and molecules (e.g., see Refs. 2–4). Its counterpart in solids has been shown both theoretically[5,6] and experimentally[7,8] to have similar sensitivity on electron correlation. The arguably most important effect where correlation between electrons plays a key role is superconductivity. Here, two electrons with opposite momentum pair up to form a bound Cooper pair. In a groundbreaking theoretical work, Kouzakov and Berakdar have demonstrated[9] that the direct emission of a Cooper pair by a single photon should be possible. They predict that the properties of the bound state are conserved upon photoejection through the surface into the continuum. This would open the road for a novel type of spectroscopy of superconductivity promising direct momentum space images of Cooper pairs on a detector. It would also give new insight into the nature of the pairing process.[10,11]

Different setups to study electrons being emitted from surfaces using coincidence measurements exist today.[12,13] These experiments use either two or more hemispherical analyzers, where the kinetic energy of each electron is measured with high resolution under a certain emission angle or position-sensitive detectors, where the time of flight is measured together with the position on several position-sensitive detectors. A different approach has been implemented by Hattass *et al.*[14] in 2004 by using only one time- and position-sensitive detector with multiple hit detection capability[15] in an approach that is based on the so called cold target recoil ion momentum spectroscopy (COLTRIMS).[16] The same kind of spectrometer has been used to study low energy electrons emitted from surfaces.[17]

In this imaging approach, all electrons which are emitted are guided by homogeneous electric and magnetic fields onto the detector. From the time of flight and position of impact on the detector, the full momentum vector of each electron can be calculated. It has been shown that this technique is well suited to address correlation effects in materials.[7] The key advantage regarding coincident electron emission is its large solid angle. The solid angle of the spectrometer is crucial, because the detection efficiency of single electrons accounts quadratically to the detection efficiency of a true coincident event. Since this emission process is very unlikely to occur, depending on the material and photon energy ranging from 1% to 3% of the total electrons emitted, the detection efficiency has to be maximized. In addition, the intensity of the incoming photon beam cannot be adjusted at will. A linear increase of the intensity leads to a quadratic enhancement of uncorrelated background, e.g., simultaneous emission of two electrons by two photons.

a)wallauer@atom.uni-frankfurt.de.

 

The application of this imaging approach to the study of superconductors requires some modifications of the technique. Magnetic fields which are in many cases used to guide the electrons onto the detector can no longer be used. The expelled field from the superconducting sample would cause distortions of the electron trajectories prohibiting the calculation of the momenta from the acquired data. Therefore, only an electric field can be applied. In order to maintain the large acceptance angle of the spectrometer, the time of flight of the electrons necessarily has to be kept short in order to make the electrons still hit the detector. This results in an increased dead-time problem since electron pairs impinge almost simultaneously on the detector. These dead-time problems can be traced back to the identification of two overlapping electronic signals and the determination of their correct time position. Therefore, we record the full waveform of the electronic pulses generated by the detector and apply various algorithms to analyze the timing of each of the overlapping pulses. We describe the application of a new algorithm to decrease the dead time significantly and moreover to enable and to quantify the influence of remaining detector dead time on the results.

## II. EXPERIMENTAL SETUP

The experimental setup consists of a vacuum chamber, which is pumped by a turbomolecular pump, a titanium sublimation pump, and a getter pump (SAES MKS 500). We achieve a base pressure of $3 \times 10^{-11}$ mbar. In this way, it is possible to measure even cooled samples with a clean surface for more than 10 h. Such long data collection times are essential for coincidence experiments.

A Pb(111) single crystal is mounted on a custom-made sample holder, which is attached to a liquid helium flow cryostat. Before the measurement, the lowest temperature at the sample position has been determined with a calibrated silicon diode to be as low as 4.5 K. This allows us to measure well below the critical temperature of Pb (7.2 K). For a comparative measurement in the non-superconducting state, the sample holder can be heated up by a resistive heating wire. Sample cleaning was performed by repeating cycles of Argon bombardment and annealing to 420 K.

The time-of-flight spectrometer is shown in Figure 1. It consists of eight copper rings, each separated from one another by a ceramic spacer of 5 mm. These electrodes are connected by resistors in order to create a homogeneous electric field inside the spectrometer volume. The angle of incidence of the photon beam is 70° to the surface normal. A stainless steel end plate with a hole of 40 mm in diameter is fitted to the outer diameter of the sample holder in order to achieve a flat spectrometer end plate, which is essential for the creation of a homogenous field. The opposite spectrometer end in front of the detector is defined by a stainless steel mesh of 250 $\mu$m with a transmission of 80%. A second mesh with same properties, separated by 6 mm and set to a slightly lower potential, has proven useful. It efficiently suppresses electrons, which are created by electron impact at the first mesh. The total length of the spectrometer is 48.7 mm (from mesh to sample) and a voltage of 35 V is applied to the

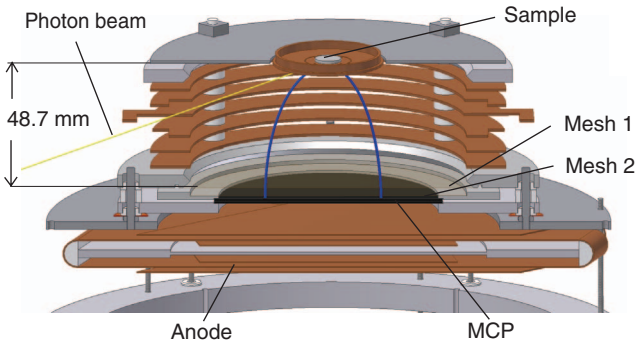


FIG. 1. Cut through the detector and spectrometer. The photon beam (yellow) is incident under 70° to the surface normal. For clarity purposes, all parts from the sample holder are removed except the sample itself and part of the shielding, which fits right into the spectrometer end plate in order to guarantee a homogeneous electric field inside the spectrometer. Two sample trajectories of emitted electrons are sketched in blue.

first mesh, creating a field of 7.2 V/cm. With these parameters, the resulting time-of-flight difference between the fastest and the slowest electrons is only around 16 ns for 25 eV photon energy.

The detector consists of a microchannel plate (MCP) stack from which the time-of-flight information is retrieved and a hexagonal delay line anode (Roentdeck HEX80)[15] from which the position can be calculated. The principle of the position measurement is described in detail in the Appendix. In short: the anode consists of three wire sets, arranged hexagonally at 120° to each other. The electron cloud leaving the MCP's induces an electronic signal running to both ends of each layer. By analyzing the arrival times of these signals, one position coordinate can be calculated per layer simply by the time difference of the signals followed by a transformation to the Cartesian coordinate system. In case more than one electron hits the detector, the sum of the run times of the signal to the two ends of each wire allows the correct assignment of the signals.

The usage of a hexagonal anode has decreased the dead-time effects significantly since it offers redundant information on the impact position. The two coordinates are obtained from three layers. Missing signals on one layer can then be reconstructed from signals on other layers and even the time of impact for the second electron, which is rarely detected by the MCP, can be retrieved. For a correct assignment of the signals to the corresponding electrons, we use an algorithm that reconstructs the time of missing signals and checks for their consistency with the timing of the measured signals.[15] This algorithm is used in all of our data analysis. The inputs to this algorithm are the arrival times of all of the pulses. In most of the applications, this time information is obtained by feeding the analog pulses of the detector into a constant fraction discriminator, which creates norm pulses used to start or stop a time-to-digital converter. A major improvement can be achieved by recording the full pulse shape by using a Flash analog-to-digital converter (ADC) and employing more sophisticated pulse-finding algorithms. We will address this pulse recognition in Sec. III.

## III. DATA ANALYSIS

### A. Data acquisition system

The analog signals of each layer of the anode, the MCP signal, and a timing signal synchronized to the light source (bunch marker) are digitized and recorded with an eight channel 8-bit digitizer (Acqiris DC-271) with a sampling rate of one GSample/s. The accurate waveforms of all signals for each event are transferred to a computer where they are stored in an event-by-event list mode file. Various algorithms such as a software constant fraction discrimination can be used later in the offline analysis software to extract the arrival times of all recorded pulses, which will then be converted into full momentum vectors for every electron of each event.

Most events where two electrons are emitted yield overlapping pulses on the MCP or the delaylines, which is the reason why those double events are much more difficult to analyze. Disentangling these pulses and retrieving their timing accurately is a major challenge. Even though corresponding algorithms might appear appropriate at first glance, they often fail for real detector signals. Storing the full waveform of every pulse allows to perform quality checks during the development of new algorithms. The functionality of this quality check is sketched in Figure 2 for one (anode) channel. Here, we randomly choose two different single photoemission events (pulses A and B, upper left and right) and analyze their arrival time and position individually. Then the raw data of both signals (red and blue) are merged for every channel to create the artificial double event X. We can then analyze the raw data pulseshape of the newly created double event X to obtain the two signals of Xa and Xb and compare their time position to A and B, respectively.

This procedure can be repeated as often as desired to create an almost infinite number of simulated double events. The comparison can than be used to retrieve not only how many simulated double events a specific routine is able to find, but also how big and of what shape the dead-time effect is in time and space. Furthermore, the merging of single photoemission events allows us to simulate very accurately the background from events where two electrons are created independently by two photons.

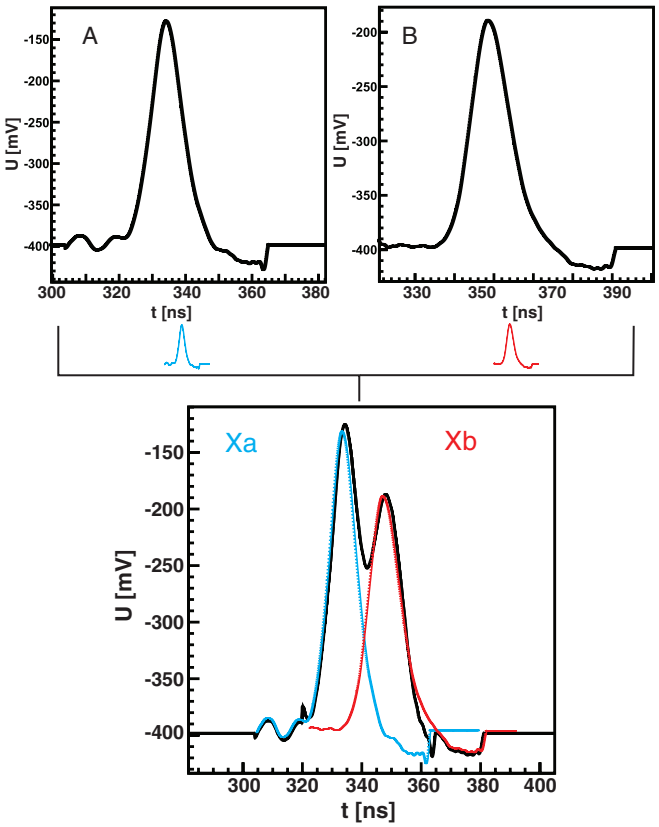


FIG. 2. Merging of two single-hit events to an artificial double-hit event with known time position of the pulses. Upper left and right panel show pulses from electrons A and B recorded from two different events. Both waveforms are added to simulate an event, where two electrons hit the detector. These artificial electrons are equivalent to electrons, which were created in the same light pulse but independently by two photons. The new event (lower panel) shows a typical double pulse (black), which can be used to test the pulse analysis algorithms. The result of this algorithm Xa and Xb can be compared to the known timing information of A and B.

### B. Pulse analysis

The position in time of single-hit pulses can be determined accurately by various algorithms, e.g., center of mass or a constant fraction (CFD) algorithm.[18,19] However, we find that for pulses coming from the delayline anode that are separated in time by less than 15 ns or pulses from the MCP that have a difference in arrival time less than 10 ns, the CFD algorithm recognizes less than 10% of the existing pulses. A new algorithm for pulse analysis has been proposed by Da Costa *et al.*[20] In this algorithm, the shape of a typical signal from a single event is determined by taking the mean of a number of signals originating from single-hit events. Then the start position of the pulse is found by a CFD algorithm. In the third step, the mean pulse is fitted to the waveform at the time position extracted from the second step. The appropriate height is determined by the slope of the leading edge of the analyzed pulse. The fitted pulse can then be subtracted from the whole waveform and the remaining signal can once again be analyzed with a CFD algorithm. This procedure is repeated until no signal remains.

By applying this algorithm, we found in the majority of the analyzed events a very good agreement between the retrieved position in time with the correct ones known from the single-hit pulses before merging the pulses. However, the algorithm can produce serious errors when the leading edge is influenced by noise or when a signal almost coincides with the following signal. Therefore, we used the time information obtained by the described algorithm only as a starting value for a slower but more robust fitting procedure. We fitted the sum of two mean signals to the original waveform using a multidimensional minimization algorithm.[21] The measure of the best match is the integrated difference of measured signal and sum of two mean signals. Height and position of each mean signal is varied until the integrated difference becomes minimal.

The improvement of detection efficiency can be seen in Figure 3 comparing the standard CFD (left) and pulse-fit (right) algorithm. Both histograms show the weighted difference of two spectra: first, the true time-of-flight and

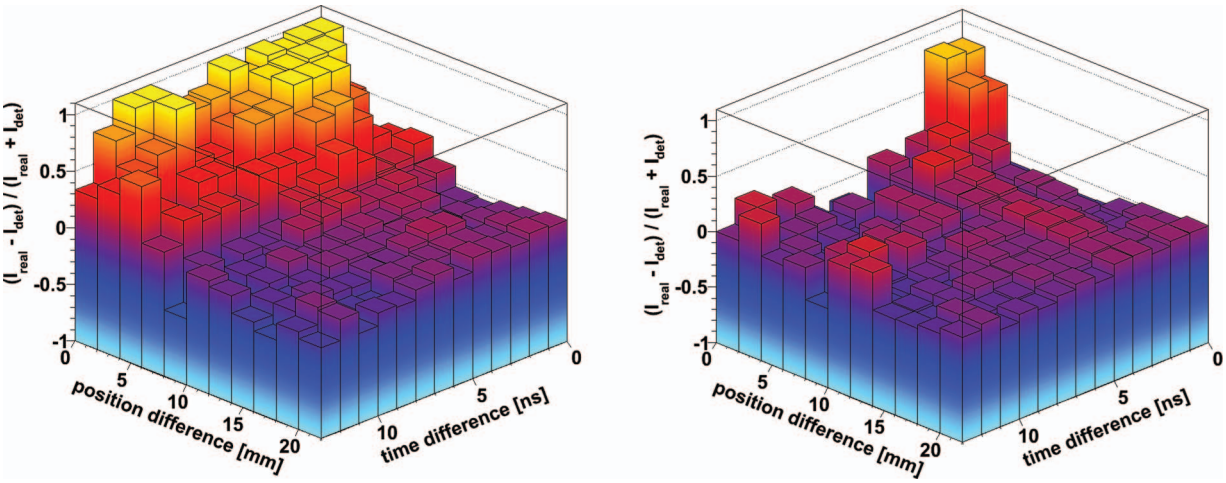


FIG. 3. Particle loss probability as a function of time- and position difference of an electron pair on the detector. The x- and y-axis show the time difference between two consecutive hits and the distance in position between the two hits. The z-axis shows the difference between the number of hits retrieved by the respective algorithm and the real number of hits in an event-mixed sample file. Both spectra are normalized to the sum of the hits. Therefore yellow color (z-axis = 1) indicates a complete loss of all events in this region, while purple (z-axis = 0) indicates a correct retrieval of all events. Negative values indicate that events have been found which are not real at this position and time, but might have been in a neighboring bin. Application of a standard CFD (left) and pulse fitting algorithm (right). See text.

position difference is calculated for two independent single-hit events. This results in a spectrum, which simulates the ideal case of two particles generated by two photons and detected without detector dead-time effects. The second spectrum is generated by using the algorithm under test to identify the pulses. The intensity in every bin is then calculated by the difference of the intensity in the ideal case $I_{real}$ and the test case $I_{det}$, divided by their sum. This way, regions where signals could not be found are shown as red to yellow colors. Both spectra show the particle loss probability as a function of position- and time-difference of the two electrons hitting the detector. As it can be seen, double events closer than 10 mm are rarely retrieved using a standard CFD algorithm. In contrast, events as close as 5 mm in position and 3 ns in time can be retrieved with our pulse-fit algorithm. Fluctuations at larger time- and position-difference stem from small shifts in the fitted time. Nevertheless, the overall efficiency in this area for two particles to be detected equals to one.

## IV. RESULTS

First, experiments have been performed at the 3m-NIM Beamline at BESSY with photon energies from 9 eV to 40 eV. In five days, we recorded around 300 million single photoemission events. A real double photoemission event appears with less than 1% probabillity (<3 million). With the new pulse-fit algorithm, we were able to increase the number of detected double events by 20%. Figure 4 shows the time-of-flight distribution of the electrons vs. their impact position on the detector for a photon energy of 30 eV. The x-position of impact is depicted on the ordinate while the y-coordinate is restricted to ±2.5 mm around the center of the detector. To illustrate the imaging properties of the spectrometer, solid lines for same emission angles and electron energies indicated in the middle are laid with the spectrum on the right.

As mentioned before, the major part of emitted electrons corresponds to the photoemission of a single electron.

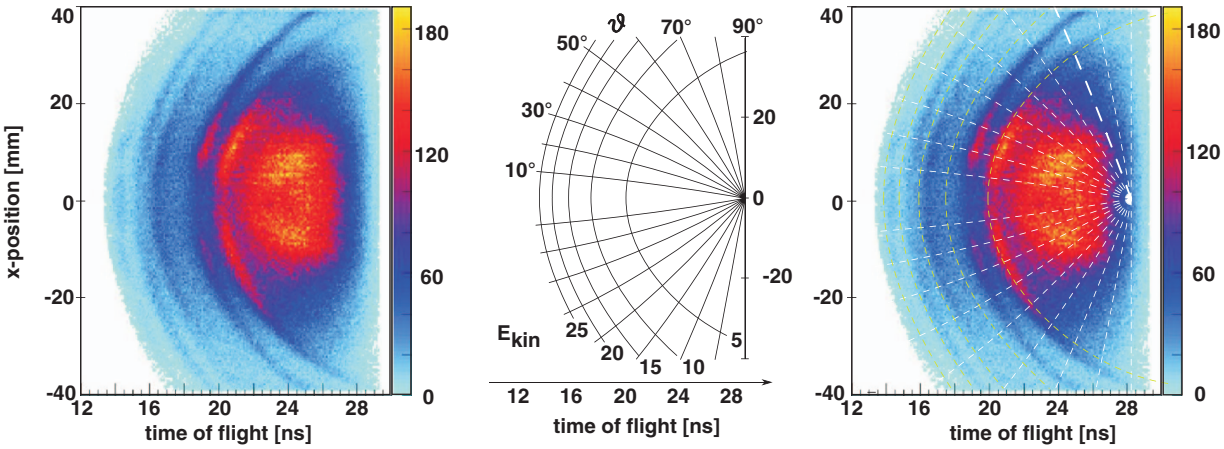


FIG. 4. (Left) Electrons from 30 eV photon impact on a Pb(111) surface detected by the spectrometer shown in Figure 1. Horizontal axis: time of flight, vertical axis: x-position of impact on the detector. Only events for which the y-position is within ±2.5 mm to the center of the detector. (Middle) Calculation of lines of same energy and emission angle for the described spectrometer and field (7.2 V/cm). (Right) Calculated lines laid with the recorded spectrum.

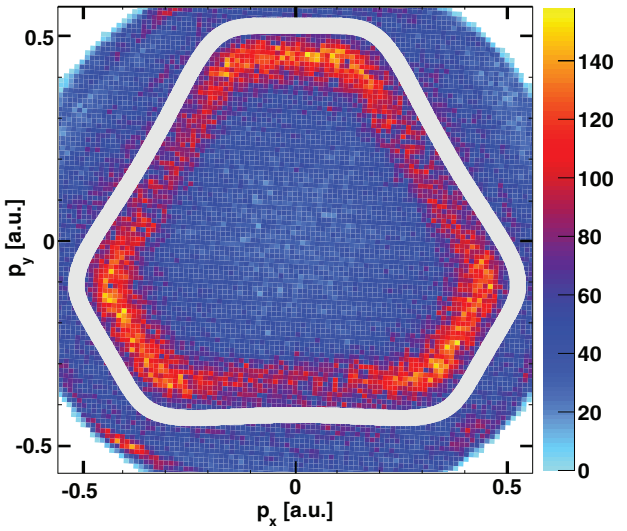


FIG. 5. Fermi surface cut of Pb(111)surface at photon energies of 9 eV. The parallel momentum of electrons with kinetic energies of ±0.25 eV around $E_F$ is shown. White line represents theoretical calculations perpendicular to $L$ at 0.85 of $\Gamma - L$ consistent with an inner potential of 11.8 eV.

These results can therefore be compared to theory and they can be used to verify the surface preparation and the spectrometer properties. To our knowledge, the only experimental data available for Pb(111) surfaces can be found in Ref. 22. Figure 5 shows the results of Fermi surface mapping at photon energies of 9 eV. The window in energy is ±0.25 eV around $E_F$. The white line represents a theoretical calculation, which corresponds to an inner potential of 11.8 eV. This is in agreement with other measurements.[22]

We theoretically determine the Fermi surface of Pb with the help of density functional theory calculations in the full potential local orbital (FPLO) basis.[23] We use the generalized gradient approximation (GGA)[24] as exchange-correlation functional and integrate the Brillouin zone with a 24 × 24 × 24 $k$ mesh. Due to the large mass of Pb, we first compared scalar relativistic and fully relativistic calculations of the electronic structure. As we found a significant influence of the spin-orbit coupling which also affects the Fermi surface, we chose to continue with fully relativistic calculations. Cuts through the Fermi surface were determined perpendicular to the $L = (\pi/a, \pi/a, \pi/a)$ direction in reciprocal space.

In case of coincident events, the quantity, where the effects of the detector dead-time on the momentum distribution are most significant, is the relative momentum of the two electrons. Therefore, we calculate the relative momentum $p_{rel}$ in the $p_x$, $p_y$-plane

$$p_{rel} = \sqrt{(p_{x1} - p_{x2})^2 + (p_{y1} - p_{y2})^2} \qquad (1)$$

and compare the results for different $\Delta p_z = |p_{z1} - p_{z2}|$, which directly reflect the time-of-flight differences. The results are shown in Figure 6 for the two used algorithms, CFD (grey curve) and pulse-fit (blue). For a better comparison, all spectra were corrected for solid angle effects by dividing the intensity by the relative momentum. It can be clearly seen that the

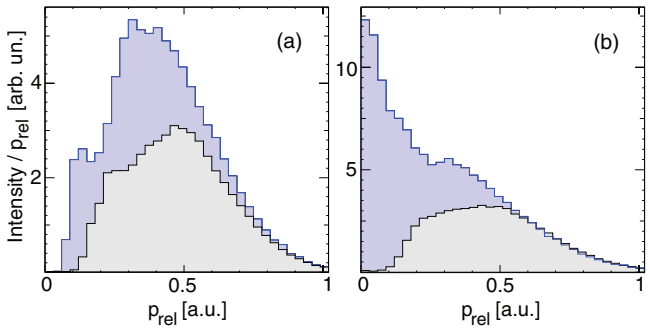


FIG. 6. Influence of detector dead time on momentum space distributions of electron pairs. Relative momenta in the $p_x$, $p_y$-plane of two electrons are compared when using the standard CFD algorithm (grey) and the pulse-fit algorithm (blue). Both spectra are corrected for solid angle effects. (Left) $p_z$ of the electrons are equal (within 0.1 a.u.). (Right) $p_z$ of the electrons differs by 0.4 ± 0.1. a.u.

usage of the pulse-fit algorithm not only leads to a significant increase of detected pairs at $\Delta p_z = 0 - 0.1$ a.u. (left) where the electrons hit the detector almost at the same time, but also for larger $\Delta p_z = 0.3 - 0.4$ a.u. (right). The difference is even bigger in the latter case, since electrons that hit the detector at the same position are still very unlikely to be found in case of the CFD algorithm.

In conclusion, an imaging spectrometer for electron pairs from cryogenically cooled surfaces has been constructed and tested. We have shown that the single-photoemission results recorded with this spectrometer are in good agreement with theoretical predictions and that it fulfills the simulated energy resolution of around 1/30. Higher energy resolutions are possible with the application of electrostatic lenses at the cost of losing solid angle. Our spectrometer is designed for large solid angles in order to look for the signature of Cooper pairs in their parallel momentum. It is predicted by theory,[9] that the sum of their parallel momentum peaks at $p_{1,\parallel} + p_{2,\parallel} = 0$. In this dimension, the spectrometer has a high resolution of around 0.01 a.u.. As a result of the special spectrometer design, the two electrons are impinging at almost the same time on the detector and dead time becomes a crucial quantity. This holds even more for the study of direct emission of Cooper pairs, where the process is expected in only a small fraction of the overall coincidence emission from the valence band. To address the problem of detection efficiency, we implemented a new pulse analysis algorithm, which reduces the phase space region in which no electron pairs can be detected by more than a factor of two.

## ACKNOWLEDGMENTS

This work is supported by the BMBF. H.O.J. acknowledges support by the Helmholtz Association via HA216/EMMI. We thank HZB for the allocation of synchrotron radiation beamtime and financial support.

## APPENDIX: SIGNAL ASSIGNMENT AND POSITION CALCULATION OF MULTIHIT EVENTS

Figure 7 shows a full set of signals recorded from an event where two electrons hit the detector at about the same

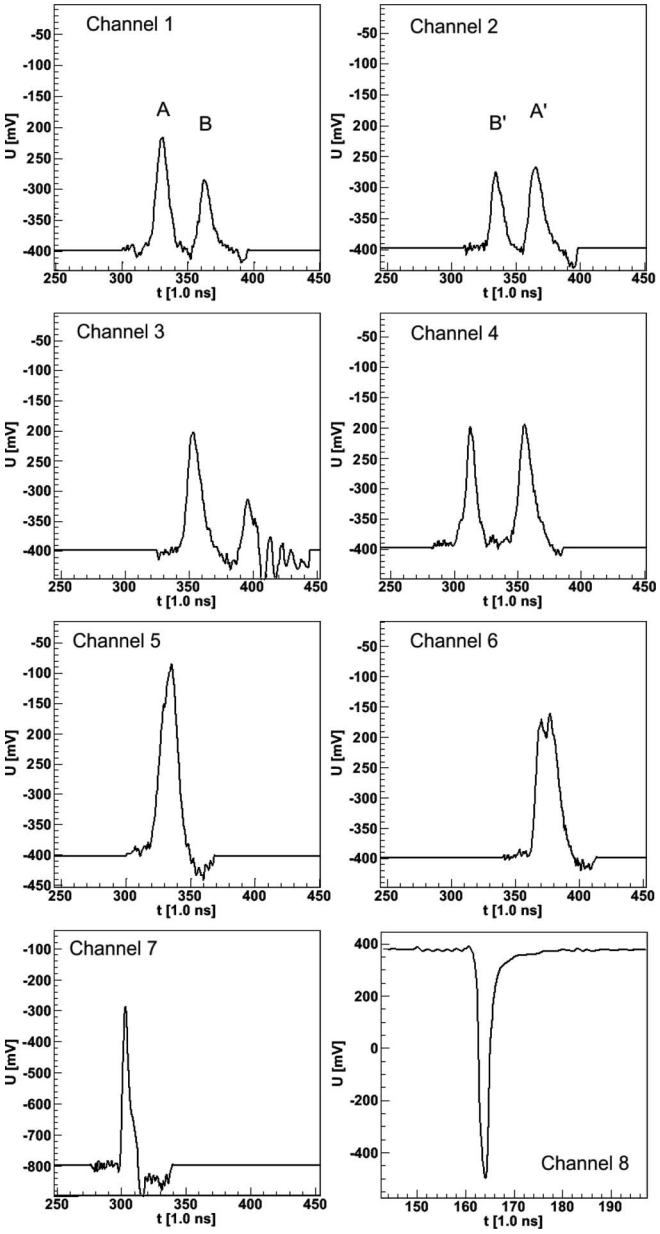


FIG. 7. All channels recorded for one event where two electrons hit the detector at about the same time. Channels 1−6 are the ends of the three anode layers, Channel 7 the MCP-signal, and Channel 8 the timing signal from the light source. Whereas signals are well separated on the first four Channels, they are strongly overlapping on Channels 5, 6, and 7. The assignment of two corresponding signals is done by calculating the time sum. A and A′ represent the pulses of the first hit, B and B′ the sum of the second hit.

time. Channels 1−6 are the six ends of the three anode layers, where each pair of consecutive Channels (1 + 2, 3 + 4, 5 + 6) represents one layer. Channel 7 is the MCP signal and Channel 8 the timing signal from the light source.

Since the electrons hit the MCP very close in time, only one MCP signal can be identified. From the time difference of the MCP and the bunchmarker signal, the time of flight of the first electron is calculated. A constant offset value has to be found via calibration. The MCP time of the second electron has to be deduced from the anode signals. First, the signals at each end have to be assigned to the correct electron hit. For this purpose, we use the runtime of the signals on the layer, which is a certain constant for each layer. Hence, the time sum $t_{sum}$ of the of two signals from one event have to be equal to that constant

$$t_{Ch_1} + t_{Ch_2} - 2 \cdot t_{MCP} = t_{sum} = const. \tag{A1}$$

As it can be seen in Figure 7, the signals corresponding to the first hit on the detector are not necessarily the first signals detected in each channel. In Channels 1 and 2, signals A and A′ correspond to the first electron, while B and B′ correspond to the second electron, respectively. The time position of the two signals A (330 ns) and A′ (365 ns) relative to the time position of the MCP (305 ns) add up to 85 ns. The time sum of the second hit will have a certain offset from this constant, in this case, around 1 ns. The small width of the time sum (around 500 ps) allows not only a correct assignment of the signals, but also a calculation of the time of the MCP signal of the second electron and thereby its time of flight.

The position of impact on each layer can be calculated by the difference of the two corresponding signals. The position on the layers is typically denoted by $u$, $v$, and $w$, so that the position on a layer is calculated by

$$u, v, w = (t_{Ch_{1,3,5}} - t_{Ch_{2,4,6}}) \cdot c_{u,v,w}, \tag{A2}$$

where c is the propagation speed on the layer perpendicular to the wiring. Its value again differs slightly for each layer, since it depends on the layers size. The two coordinates $x$ and $y$ can then be calculated from any two of the three layers[15]

$$x_{uv} = u, \qquad y_{uv} = \frac{u - 2v}{\sqrt{3}}, \tag{A3}$$

$$x_{uw} = u, \qquad y_{uw} = \frac{2w - u}{\sqrt{3}}, \tag{A4}$$

$$x_{vw} = v + w, \qquad y_{vw} = \frac{w - v}{\sqrt{3}}. \tag{A5}$$

The redundant information on the position is used not only to perform consistency checks in the assignment of signals, but also to correct for non-linearities in the position calculation.

[1] J. S. Briggs and V. Schmidt, J. Phys. B **33**, R1 (2000).
[2] T. Weber, H. Giessen, M. Weckenbrock, G. Urbasch, A. Staudte, L. Spielberger, O. Jagutzki, V. Mergel, M. Vollmer, and R. Dörner, Nature (London) **405**, 658 (2000).
[3] W. Vanroose, F. Martín, T. N. Rescigno, and C. W. McCurdy, Science **310**, 1787 (2005).
[4] D. Akoury, K. Kreidi, T. Jahnke, T. Weber, A. Staudte, M. Schöffler, N. Neumann, J. Titze, L. P. H. Schmidt, A. Czasch, O. Jagutzki, R. A. Costa Fraga, R. E. Grisenti, R. Díez Muiño, N. A. Cherepkov, S. K. Semenov, P. Ranitovic, C. L. Cocke, T. Osipov, H. Adaniya, J. C. Thompson, M. H. Prior, A. Belkacem, A. L. Landers, H. Schmidt-Böcking, and R. Dörner, Science **318**, 949 (2007).
[5] J. Berakdar, Phys. Rev. B **58**, 9808 (1998).
[6] N. Fominykh, J. Berakdar, J. Henk, and P. Bruno, Phys. Rev. Lett. **89**, 086402 (2002).
[7] M. Hattass, T. Jahnke, S. Schössler, A. Czasch, M. Schöffler, L. Schmidt, B. Ulrich, O. Jagutzki, F. Schumann, C. Winkler, J. Kirschner, R. Dörner, and H. Schmidt-Böcking, Phys. Rev. B **77**, 165432 (2008).
[8] F. Schumann, C. Winkler, and J. Kirschner, Phys. Rev. Lett. **98**, 257604 (2007).
[9] K. Kouzakov and J. Berakdar, Phys. Rev. Lett. **91**, 257007 (2003).

[10]K. Kouzakov and J. Berakdar, J. Electron Spectrosc. Relat. Phenom. **161**, 121 (2007).
[11]B. D. Napitu and J. Berakdar, Phys. Rev. B **81**, 195108 (2010).
[12]R. Gotter, A. Ruocco, A. Morgante, D. Cvetko, L. Floreano, F. Tommasini, and G. Stefani, Nucl. Instrum. Methods Phys. Res. A **467-468**, 1468 (2001).
[13]F. O. Schumann, C. Winkler, and J. Kirschner, Phys. Status Solidi B **246**, 1483 (2009).
[14]M. Hattass, T. Jalowy, A. Czasch, T. Weber, T. Jahnke, S. Schossler, L. Ph. Schmidt, O. Jagutzki, R. Dörner, and H. Schmidt-Böcking, Rev. Sci. Instrum. **75**, 2373 (2004).
[15]O. Jagutzki, A. Cerezo, A. Czasch, R. Dorner, M. Hattas, V. Mergel, U. Spillmann, K. Ullmann-Pfleger, T. Weber, H. Schmidt-Bocking, and G. Smith, IEEE Trans. Nucl. Sci. **49**, 2477 (2002).
[16]R. Dörner, V. Mergel, O. Jagutzki, L. Spielberger, J. Ullrich, R. Moshammer, and H. Schmidt-Böcking, Phys. Rep. **330**, 95 (2000).
[17]P. Kirchmann, L. Rettig, D. Nandi, U. Lipowski, M. Wolf, and U. Bovensiepen, Appl. Phys. A **91**, 211 (2008).
[18]L. M. Foucar, "Auslese von Delaylinedetektoren mit Hilfe von Transientenrekordern," Ph.D. dissertation (Goethe-Universität, Frankfurt, 2008).
[19]K. Motomura, L. Foucar, A. Czasch, N. Saito, O. Jagutzki, H. Schmidt-Böcking, R. Dörner, X.-J. Liu, H. Fukuzawa, G. Prümper, K. Ueda, M. Okunishi, K. Shimada, T. Harada, M. Toyoda, M. Yanagihara, M. Yamamoto, H. Iwayama, K. Nagaya, M. Yao, A. Rudenko, J. Ullrich, M. Nagasono, A. Higashiya, M. Yabashi, T. Ishikawa, H. Ohashi, and H. Kimura, Nucl. Instrum. Methods Phys. Res. A **606**, 770 (2009).
[20]G. Da Costa, F. Vurpillot, A. Bostel, M. Bouet, and B. Deconihout, Rev. Sci. Instrum. **76**, 013304 (2005).
[21]M. Galassi, J. Davies, J. Theiler, B. Gough, G. Jungman, P. Alken, M. Booth, and F. Rossi, *GNU Scientific Library Reference Manual* (Network Theory Limited, 2011).
[22]K. Horn, B. Reihl, A. Zartner, D. Eastman, K. Hermann, and J. Noffke, Phys. Rev. B **30**, 1711 (1984).
[23]K. Koepernik, Phys. Rev. B **59**, 1743 (1999).
[24]J. P. Perdew, K. Burke, and M. Ernzerhof, Phys. Rev. Lett. **77**, 3865 (1996).